RSC Advances

ROYAL SOCIETY OF CHEMISTRY

www.rsc.org/advances

A fast and simplified synthesis of cuprous oxide nanoparticles: anneal studies and photocatalytic activity

Liangbin Xiong,[*ab] Huaqing Xiao,[a] Shunsheng Chen,[c] Zhihong Chen,[a] Xunong Yi,[a] Sheng Wen,[d] Genwen Zheng,[d] Yaoming Ding[a] and HuaqingYu[a*]

[a]*School of Physics and electronic-information Engineering, Hubei Engineering University, Xiaogan, 432000, China.*

[b]*Key Laboratory of Artificial Micro- and Nano-structures of Ministry of Education of China, School of Physics & Technology, Wuhan University, Wuhan, Hubei 430072, P. R. China.*

[c]*The Institute for Quantum materials and School of Mathematics and Physics Hubei Polytechnic University, Huangshi, P. R. China, 435003, China.*

[d]*College of Chemistry and Materials Science, Hubei Engineering University, Xiaogan 432000, China*

[*]Corresponding authors: Tel: +86 712 2345 441, E-mail: xiong_lb@yahoo.com (L.B. Xiong); and Tel: +86 712 2345 441, E-mail: yuhuaqing@126.com (H.Q. Yu)

Abstract Art

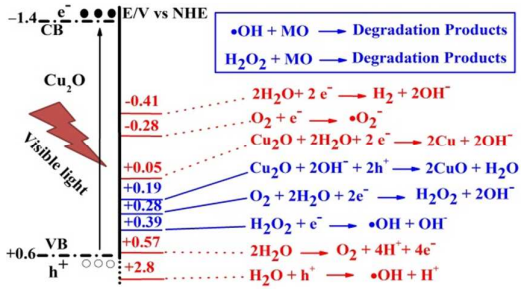

Cu_2O nanoparticles synthesized by using a fast and simplified method show a superior photocatalytic activity towards methyl orange.

RSC Advances

RSCPublishing

ARTICLE

A fast and simplified synthesis of cuprous oxide nanoparticles: anneal studies and photocatalytic activity

Cite this: DOI: 10.1039/x0xx00000x

Liangbin Xiong,*[ab] Huaqing Xiao,[a] Shunsheng Chen,[c] Zhihong Chen,[a] Xunong Yi,[a] Sheng Wen,[d] Genwen Zheng,[d] Yaoming Ding[a] and Huaqing Yu*[a]

Received 00th January 2012,
Accepted 00th January 2012

DOI: 10.1039/x0xx00000x

www.rsc.org/

We synthesized highly (111) plane oriented cuprous oxide (Cu_2O) nanoparticles (NPs) by a fast and simplified chemical deposition method with an inorganic process at ambient temperature. The variations of crystal structure parameters, morphology, energy bands, and Bruauer-Emmett-Teller (BET) surface areas were recorded for Cu_2O NPs at different annealing temperatures under N_2 atmosphere. A phase coexistence of Cu_2O and Cu was observed after the Cu_2O NPs was annealed at 600 ℃ for 2 h under N_2 atmosphere. The Cu_2O NPs show high BET surface areas and a blue shift of absorption edge in comparison with Cu_2O microparticles. We observed a superior photocatalytic activity for the degradation of methyl orange (MO) by Cu_2O NPs, which reached 100% in 55 min with as high as 7.26 $mg•min^{-1}g^{-1}$ of decolorization rate. However, Cu_2O NPs are more vulnerable to photocorrosion than Cu_2O microparticles. The mechanisms of photocatalysis for Cu_2O under visible light were also discussed in detail. Hydrogen peroxide and hydroxyl radical were found responsible for the decolorization of MO.

1. Introduction

Cuprous oxide (Cu_2O) nanoparticles (NPs) are widely used as antiseptic, germicide, catalyzer and colorant in daily life [1, 2]. It is also a promising material for photo-electricity transition [3, 4], cathode of lithium ion cell [5], and photon sensing [6]. In recent years, Cu_2O NPs have been found to be a stable photocatalyst particularly applied for hydrogen generation [7, 8] and degradation of organic contamination under visible light (VL) [9]. Thus, it is still highly of interest to synthesize Cu_2O NPs not only for the development of synthetic strategies, but also for the examination of their properties.

Various preparation methods for Cu_2O NPs [10-15] have been developed. In these methods for forming Cu_2O NPs, organic compounds are frequently used as the precursor [15] or as surfactant and template for preventing aggregation and controlling size as well as morphology [10-14]. However, the use of organics often inhibits the progress of photocatalytic (PC) reaction due to the covering of Cu_2O by surfactant [16]. Furthermore, Cu_2O NPs with highly ordered nanostructures have attracted much attention due to their novel properties in photocatalysis and stability in recent years. (111) plane of Cu_2O was found to show superior PC activity [17, 18] and Cu_2O exposing (111) facets could be used as a stable photocatalyst [19-21]. Therefore, the fabrication of Cu_2O NPs with preferentially oriented (111) facets by using inorganics precursors has become an important issue.

Recently, we reported a chemical synthesis of Cu_2O films with periodic pattern transfer by using a chemical bath (at 65 ℃) deposition technology [22]. In present work, this deposition technology was improved and a fast and simplified synthesis of Cu_2O NPs with preferentially oriented (111) facets was successfully achieved at ambient temperature without energy demand, complicate apparatus, any organic compounds and surfactants. Particularly, we attempted to investigate the effect of heating Cu_2O under inert atmosphere on its morphology, optical properties, stability and PC activity since no study has been carried out on this so far and heating Cu_2O in air could cause a conversion of Cu_2O to CuO [23-25]. Finally, the behaviors of adsorption, photocatalysis and stability of unannealed and annealed Cu_2O were investigated and the mechanisms of Cu_2O for PC degradation of methyl orange (MO) under VL were discussed in detail.

2. Experimental section

2.1 Materials

Copper (II) sulfate ($CuSO_4•5H_2O$, 98.0% purity), sodium thiosulfate ($Na_2S_2O_3$, 99.0% purity), sodium hydroxyl (NaOH, 99% purity) and MO (85% purity) was obtained from Sinopharm (China) and used as purchased. 2,3-bis(2-methoxy-4-nitro-5-sulfophehyl)-2*H*-tetrazolium-5-carboxanilide (XTT) (>98% purity), terephthalic acid (TA) (98% purity), horseradish peroxidase (POD) (activity: 250~330 units/mg solid), and N,N-

diethyl-*p*-phenylenediamine (DPD) (97% purity) were received from Sigma-Aldrich and used without further purification. The solutions used in this work were prepared with deionized water further purified with a Millipore Milli-Q (Millipore, Bedford, Ma, USA) purification system (resistivity ≥ 18.2 MΩ).

2.2 Synthesis of Cu_2O NPs

A stock colorless 500 mL solution of mixture was prepared by adding 400 mL of 1 M $Na_2S_2O_3$ to 100 mL of 1 M $CuSO_4$ solution. The same volume (500 mL) of 1 M NaOH solution was placed in another beaker. The mixture was poured into the 1 M NaOH solution with vigorous stir. The Cu_2O powder was obtained by centrifugation and drying. Subsequently, the Cu_2O powder was divided into equal six parts, five of which were annealed at 200, 300, 400, 500 and 600 ℃ at N_2 atmosphere with a flow rate of 35 sccm, respectively. The unannealed Cu_2O powder and those annealed at 200, 300, 400, 500 and 600 ℃ were named after sample 1, 2, 3, 4, 5, and 6, respectively.

2.3 Characterization

The phase purity of all samples was characterized by x-ray powder diffraction (XRD) using an x-ray diffractometer (Y-2000) with Cu Kα radiation (λ=1.5418 Å). A scan efficiency of $0.1\,°S^{-1}$ was applied to record the powder patterns in the range of $20° \le 2\theta \le 80°$. Scanning electron microscopy (SEM) images were obtained on a JEOL SM-6700F microscope operated at 5 kV. X-ray photoelectron spectroscopy (XPS) analyses were performed on a PHI-1600 ESCA spectrometer (USA) using 300 W Mg Kα radiation, and the binding energies were referenced to the C1s line at 285 eV from adventitious carbon. Transmission electron microscopy (TEM) and high-resolution transmission electron microscopy (HRTEM) were carried out with JEOL JEM-100CXII. The Brunauer-Emmett-Teller (BET) surface areas of the samples were determined by a high speed automated area and pore size analyzer (NOVA 2000e).

2.4 Adsorption and PC activity measurement

The liquid phase degradation of MO was used as a model reaction to evaluate the PC activity for Cu_2O powder. In a typical PC experiment, 0.1 g catalyst was dispersed in 400 mL of 100 mg/L MO solution. Prior to irradiation, the suspension was then sonicated for 30 min in dark to ensure the catalyst disperse well in the solution and the establishment of the adsorption/desorption equilibrium of the dye onto the surface of photocatalyst. PC reactions were conducted in a cylindrical quartz reactor with circulation water to keep the reaction temperature of 25 ℃. The equilibrium dye concentration was used as the initial concentration of the dye solution to calculate degradation efficiency. Subsequently, the suspension was transferred to the reactor. A 300 W xenon lamp (Shanghai Lansheng Ltd., Shanghai) was used as a visible-light source. A UV cutoff filter (λ < 400 nm) was used to ensure VL irradiation. The light intensity was measured by a light meter (LI-COR, USA), and the light intensity for the experiments was fixed at 1800 mW/cm^2. Aeration was performed by an air pump to ensure a constant supply of oxygen and to accomplish stirring the solution with the photocatalyst during photoreaction. At given irradiation time intervals, the liquor of 5 ml was sampled and centrifuged at 4500 rpm for 15 min to remove the photocatalyst. The MO concentration was analyzed by recording variations of the absorption band maximum at 465 nm (defined as A_t) in the UV-Vis spectra of MO by using UV-vis spectrophotometer (UV-1700, SHIMADZU). The adsorption extent R_a of the MO on the photocatalyst was determined by the MO concentration difference between the original solution (defined as A_0) and the filtrate of the MO/photocatalyst suspensions (defined as A'_0). The adsorption extent R_a of the dye on the photocatalyst was $R_a=(A_0-A'_0)/A_0\times100\%$. The degradation efficiency (R_d) of MO was calculated by the following equation: $R_d=(A'_0-A_t)/A'_0\times100\%$. The PC activity of all Cu_2O samples was detected by the method. In addition, the decolorization rates were also calculated according to following equation: $R_{dec}=V_0C_0/Q_0T\times100\%$ (unit: $mg\cdot min^{-1}g^{-1}$), where R_{dec} is the decolorization rate; V_0, C_0, Q_0, and T are the volume of suspension with MO and catalyst, initial concentration of MO, the amount of catalyst, and the time for PC reaction, respectively. Thus, here, decolorization rate is used to characterize how much dye can be discolored by a given amount of catalyst in a given time. We did this for an attempt to have a rough comparison between the PC activity of as-prepared Cu_2O with that of publications.

2.5 Measurement of hydroxyl, hydrogen peroxide and superoxide radicals

Hydroxyl radical ($^{\bullet}OH$) was detected by a photoluminescence (PL) method by using TA as a probe molecule [26]. TA readily reacts with $^{\bullet}OH$ to produce a highly fluorescent product, 2-hydroxy-TA (TA-$^{\bullet}OH$), which was measured by an Infinite M200 fluorescence spectrophotometer (Tecan, Switzerland) at emission wavelength 425 nm with excitation wavelength at 315 nm. Experimental procedure was similar to the PC measurement except that the MO aqueous solution was replaced with 4×10^{-4} M TA and 2×10^{-3} M NaOH. Superoxide radical ($^{\bullet}O_2^-$) was measured by XTT [27], which can be reduced by $^{\bullet}O_2^-$ to form XTT-formazan. The formazan has an absorption spectrum (measured by UV-1700, SHIMADZU) with a peak at 470 nm that can be used to quantify the relative amount of $^{\bullet}O_2^-$ present. Experimental procedure was similar to the PC measurement except that the MO was replaced with 1×10^{-4} M XTT. H_2O_2 was analyzed photometrically by the POD-catalyzed oxidation product of DPD [28, 29], which was measured by UV/Vis spectrophotometer (UV-1700, SHIMADZU) at 551 nm. The experimental procedure was as follows: 1) 0.3 mL of phosphate buffer (0.5 M Na_2HPO_4 and NaH_2PO_4) was added to 2.7 mL of water/sample in cuvette and mixed; 2) 50 μL of DPD reagent and 50 μL of POD reagent were added in rapid succession and mixed for 10 s; 3) The absorption spectrum 500-620 nm of the solution was taken. Water with addition of buffer and DPD reagent was used as blank.

3. Results and discussion

3.1 Characterization of Cu_2O

Cu_2O NPs were synthesized through the reduction of blue copperas ($CuSO_4\,5H_2O$) by $Na_2S_2O_3$ as the reducing agent at ambient temperature in an alkaline aqueous solution. A colorless solution of copper thiosulfate complex was formed after an overdose of $Na_2S_2O_3$ solution was added into the blue copperas solution by the following complexation equilibrium:

$$2Cu^{2+} + 4S_2O_3^{2-} \rightarrow 2\,[CuS_2O_3]^- + [S_4O_6]^{2-} \quad (1)$$

In the solution of copper thiosulfate complex, free Cu^+ ions were formed by the dissociation equilibrium [30]:

$$[CuS_2O_3]^- \rightarrow Cu^+ + S_2O_3^{2-} \quad (2)$$

After the solution of copper thiosulfate complex was poured into the NaOH solution, a yellow precipitate appeared almost simultaneously, suggesting the generation of Cu_2O. The

formation of the precipitate could be simply expressed as the reaction of free Cu^+ ions with OH^- ions:

$$2Cu^+ + OH^- \rightarrow Cu_2O + H^+ \quad (3)$$

Figure 1a shows the XRD spectra obtained in situ for samples 1-5. Five peaks at 2θ = 29.78°, 36.56°, 42.39°, 62.51° and 73.46° could be indexed to (110), (111), (200), (220) and (311) planes of the cubic phase Cu_2O with lattice constant α = 0.4266 nm, which is very close to the values in JCPDS–International Centre for Diffraction Data (PDF, Powder Diffraction File, No. 05–0667, 1996). The XRD spectrum of sample 1 (unannealed Cu_2O) is as good as the sample 2, indicating that heating Cu_2O at 200 ℃ under N_2 atmosphere did not change its phase composition. Neither other peaks of impurities nor significant change for the locations of the peaks in XRD spectra can be detected after the heat treatments, indicating pure Cu_2O powders were obtained under current synthetic conditions.

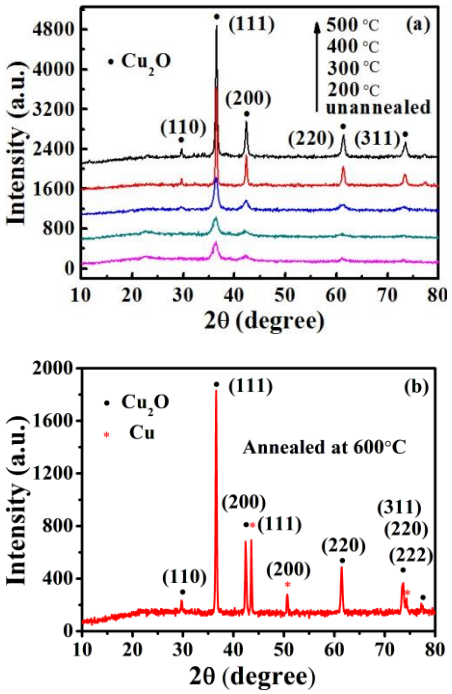

Figure1. XRD patterns of (a) Cu_2O NPs annealed at 200, 300, 400 and 500 ℃, and (b) 600 ℃ in N_2 atmosphere for 2 h.

It can also be seen from the Figure 1a, as the increase of annealing temperature, the intensity of all of the diffraction peaks increases, but their full width at half maximum (FWHM) decreases. It was well known that the width of diffraction peak will increase with the decrease of size of crystalline grain. The relation of the FWHM of diffraction peak (Δ(2θ)) and the size of crystalline grain (D) can be expressed as Debye-Scherre formula: $D = 0.89\lambda/\Delta(2\theta)\cos\theta$, where λ is the wavelength of incident ray (Cu Kα, λ = 1.5418 Å) of x-ray diffractometer. Thus, according to the FWHM of the diffraction peaks of (111) plane of Cu_2O, the average Cu_2O crystal sizes for samples 1-5 can be estimated as 7.73 nm, 7.73 nm, 9.39 nm, 21.91 nm, and 26.29 nm, respectively, indicating that the crystallinity of Cu_2O was increased with increasing annealing temperature. The heat-induced growth of crystallite of Cu_2O contributes to the increase of crystallinity because higher ordering in the structure of Cu_2O makes X-ray peak to be sharper and narrower. The peak at 36.56° was always dominant in all annealing temperature, indicating that these Cu_2O samples have highly oriented (111) planes. The numerical information of the peak height/area ratio of planes (111) and (200) for samples 1-5 are provided in Table S1, respectively. A gradually increasing peak height/area ratio of (111) plane indicates the formation of more highly oriented (111) planes with increasing annealing temperature. The formation of highly (111) plane oriented Cu_2O NPs were also confirmed by the examination of HRTEM and corresponding selected-area electron diffraction (SED) pattern. Figure 2a indicates the Cu_2O NPs was composed of rod-like and sphere-like nanostructures. One Cu_2O nanorod in the square area in Figure 2a was enlarged and shown in Figures 2b, in which the non-uniform contrast of the image indicates nanocrystalline particles with diameters of about 5-10 nm in the nanorods. The interplanar spacing of the lattice fringes in the HRTEM image of the Cu_2O nanorod (Figure 2b) is about 0.2412 nm, which corresponds to the (111) plane of the Cu_2O NPs [22]. The brighter circle corresponding to (111) plane than the others in the SED pattern (Fig. 2c) of the whole image (Figure 2b) also indicating the formation of highly (111) plane oriented Cu_2O NPs.

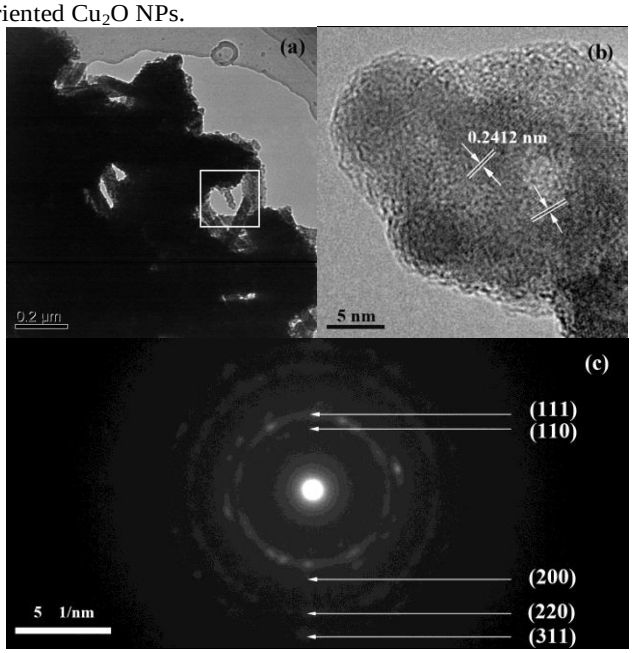

Figure 2 (a) TEM, (b) HRTEM images and (c) selected-area electron diffraction pattern corresponding to the whole image (b) area for unannealed Cu_2O NPs.

Figure 3 records a representative panoramic view of samples 2-5, from which the variation of morphology of Cu_2O with the annealing temperatures was observed. The SEM image of sample 1 was similar to the sample 2 (not shown here), indicating that the morphology of Cu_2O did not change when annealed at 200 ℃. The result is in well agreement with our XRD data and Paracchino A.'s report that heating Cu_2O to 250℃ in a N_2 atmosphere did not change the morphology of the film [23]. However, as annealing temperature increased, Cu_2O NPs with rod-like and sphere-like nanostructures disappeared, and the original Cu_2O NPs grew into large architectures with sizes ranging from several hundred of nanometers to several micrometers (Figures 3a-d and a′-d′), suggesting that annealing over 300℃ significantly influences the morphology and size of Cu_2O. Interestingly, when Cu_2O NPs was annealed at 600 ℃, a phase coexistence of Cu_2O and Cu was observed due to the

appearance of four additional peaks 2θ = 43.2°, 50.4° and 74.1° corresponding to the plane (111), (200) and (220) of copper (JCPDS card No.04-0836) [31] and the other one at 77.25° corresponding to the plane (222) of Cu_2O (Figure 1b). The heat treatment in N_2 atmosphere at 600 ℃ therefore caused the decomposition of Cu_2O (Equation 4).

$$2Cu_2O \rightarrow Cu + O_2 \quad (4)$$

3.2 Optical property of Cu_2O

Figure 4a shows the optical absorption spectra for samples 2 and 5. To estimate optical absorption edges for these two samples, the $(\alpha h\nu)^{1/n}$ versus $h\nu$ curves were plotted (Figure 4b) for n values (n = 1/2), a direct optical transition [32]. Here, α is optical absorption coefficient calculated from absorption

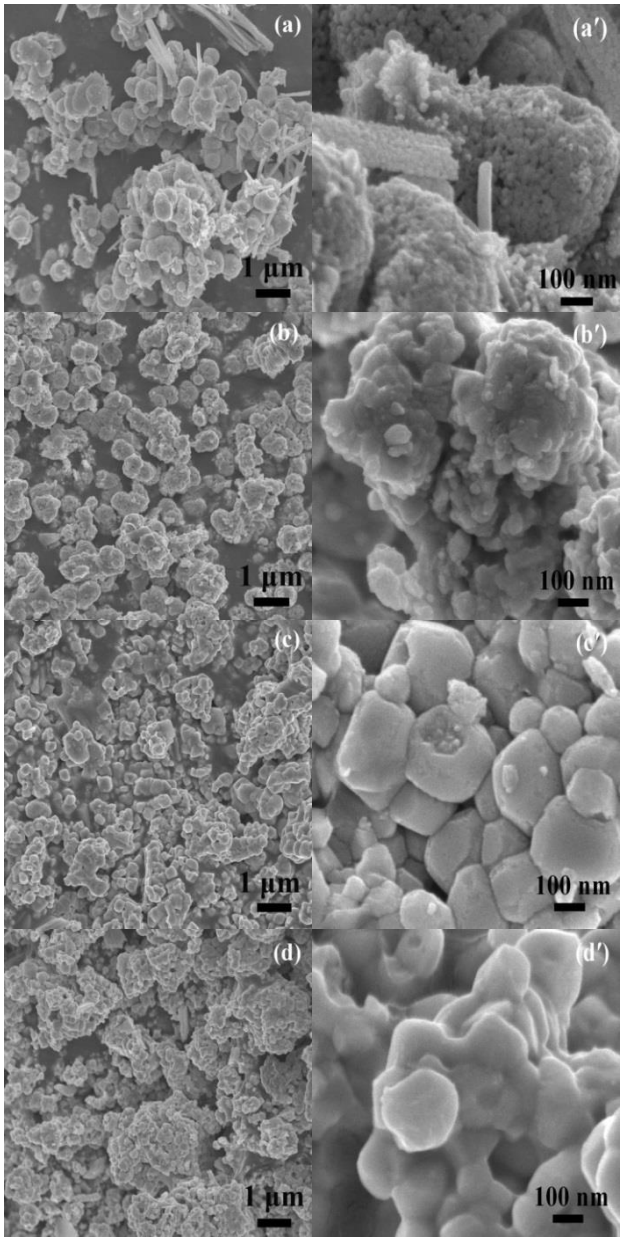

Figure 3 SEM images of Cu_2O NPs annealed at (a) 200, (b) 300, (c) 400 and (d) 500 ℃ and their enlarged images (a′), (b′), (c′), and (d′), respectively.

spectra and h is incident photon energy. The band gaps estimated for samples 2 and 5 are 2.15 and 2.10 eV, respectively, which are in agreement with literature value of 2.1 eV for Cu_2O bulk crystal [33]. The absorption edge wavelengths for samples 2 and 5 were estimated to 577 and 590 nm according to their band baps, respectively, indicating a substantial red shift for the absorption of sample 5 in comparison with that of sample 2. The UV-Vis diffuse reflectance spectra and their corresponded $(\alpha Ep)^2$ vs Ep curves of samples 1, 3, and 4 were given in Figure S2. The band gaps of samples 1, 3 and 4 were also calculated by the same method (see Table 1). The studies indicate that the band gaps of Cu_2O NPs decreases with increasing annealing temperature. We observed that the colors of the samples 2-5 generally changed from dark yellow to orange (see Table 1 and Figure S1 in Supporting Information), also suggesting the variation of optical absorption with different annealing temperature.

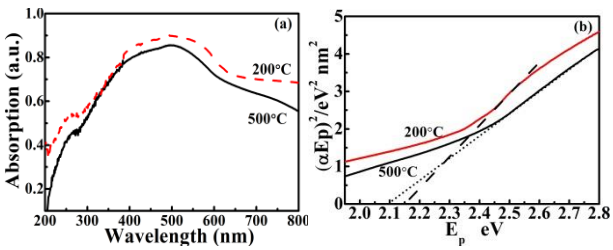

Figure 4 (a) the UV-vis diffuse reflectance spectra for Cu_2O NPs annealed at 200 and 500 ℃, and (b) their corresponding $(\alpha E_p)^2$ vs E_p curves, respectively.

Table 1 The crystal size, band gap, BET surface area, color, adsorption extent (R_a), and decolorization rates of unannealed Cu_2O NPs, Cu_2O NPs annealed at 200, 300, 400 and 500 ℃.

Samples	1	2	3	4	5
BET surface area (m^2/g)	21.63	21.37	6.156	5.521	3.011
Crystal Size (111) (nm)	7.73	7.73	9.39	21.91	26.29
Band gap (eV)	2.15	2.15	2.12	2.11	2.10
Color	Dark yellow	Dark yellow	yellow	light orange	orange
Adsorption Extent (R_a)	39.1%	38.4%	11.4%	9.6%	5.7%
Decolorization Rate (R_{dec})*	7.26	6.67	3.27	2.77	1.70

*The unit of decolorization rate is mg $min^{-1}g^{-1}$. The time for calculating decolorization rates of samples 1-5 are 55, 60, 120, 120 and 120 min, respectively. The decolorization rate is an overall averaged rate for each sample in a given time.

3.3 PC activity of Cu_2O

The adsorption extent (R_a), decolorization ratio and degradation efficiency of MO for Cu_2O samples were given in Table 1 and Figure 5, respectively. Samples 1 and 2 show a close adsorption extent, decolorization rate and degradation efficiency, indicating that annealing treatment for Cu_2O NPs at 200 ℃ did not significantly affected the its adsorption and PC activity towards MO. However, as the annealing temperature increased, these Cu_2O samples showed a diminishing adsorption extent and PC activity. The much higher degradation efficiency of samples 1 and 2 than other Cu_2O samples may be ascribed to their small particle sizes, which can increase their adsorption

ability and thereby improve their PC activity. Moreover, the small size of photocatalyst can result in more efficient transfer of photogenerated charges to the surface, also contributes to the efficient PC reaction whereas the aggregation of the photocatalyst particles involved a decrease in specific surface area as well as a change in the light scattering property of the particles [34], resulting in the degradation of PC efficiency [35]. Moreover, the higher decolorization rates of samples 1 (7.26 mg $\cdot min^{-1}g^{-1}$) and 2 (6.67 mg $\cdot min^{-1}g^{-1}$) (see Table 1) than the reported values of 6 [36], 2.75 [37] and 0.238 [12] mg $\cdot min^{-1}g^{-1}$, further indicating the superior PC activity of Cu_2O NPs towards MO.

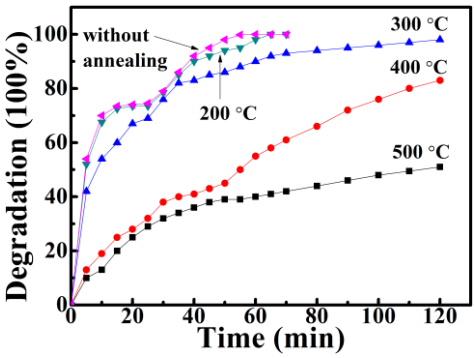

Figure 5 Degradation efficiencies of MO for unannealed Cu_2O NPs, Cu_2O NPs annealed at 200, 300, 400 and 500 ℃ under VL. 0.1 g catalyst was dispersed in 300 mL of 100 mg/L MO solution.

3.4 Stability of Cu_2O

The stability of the Cu_2O samples was investigated by comparing the structures, valence states of the Cu_2O samples before and after PC experiments. Figure S3 shows XRD patterns of samples 2-5 before and after PC experiments. The XRD pattern of sample 1 was similar to that of sample 2 after PC experiment (not shown here). Two new peaks at $2\theta = 38.73°$ and 48.65 ° corresponding to (111) and ($\bar{2}$02) planes of tenorite phase CuO (PDF, Powder Diffraction File, No. 02-1040) appeared in the XRD patterns of both sample 2 and 3, indicating they were partly oxidized into CuO during the PC process. However, no obvious change could be observed for the XRD patterns of samples 4 and 5, indicating that annealing at a higher temperature contributed to a better stability for Cu_2O.

XPS spectra were recorded to monitor the valence states of the Cu_2O samples before and after PC experiments. Figure 6a shows a representative XPS spectrum for samples 1-5 before PC experiments. It is hard for the peak to be simulated since the peak is not so broad and there is no shoulder peak. The binding energy of Cu*2p* (932.9 eV) is the same as the standard binding energy of Cu*2p* in Cu_2O, indicating that samples 1-5 were prepared as pure Cu_2O, which is well in agreement with the XRD data. Figures 6b and c show the XPS spectra of sample 1 and sample 5 after PC experiments, respectively. The XPS spectra of samples 2, 3 and sample 4 after PC experiments were similar as Figures 6b and c, respectively. All the similar data are not shown here. XPS spectra of both Figures 6b and c show a broad peak simulated with Gaussian equation, which leads to two split peaks. According the cited publication [38], the $Cu2p_{3/2}$ level of Cu_2O is narrow (FWHM = 2.0 ±0.1 eV) and has a binding energy of 933.05 ±0.75 eV while that of CuO is broad (FWHM = 2.85 ±0.25 eV) with a binding energy of 935.2 ±0.35 eV. A detailed description for the binding energies, FWHM and relative contents of different peaks for sample 1 and sample 5 after the PC experiments are listed in Table 2.

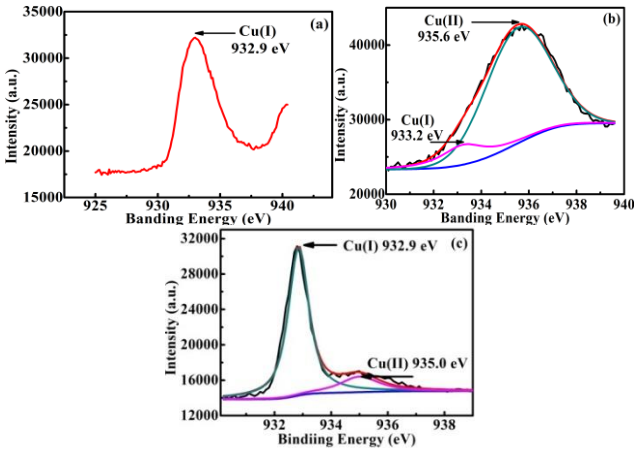

Figure 6 (a) a representative XPS spectrum of samples 1-5 before PC experiments; XPS spectra of (b) sample 1, and (c) sample 5 after PC experiments.

Table 2 The binding energies, FWHM, relative contents and area ratio of different peaks of unannealed Cu_2O and Cu_2O NPs annealed at 500℃ after the PC experiments.

Sample	1		5	
Peaks	Cu^+	Cu^{2+}	Cu^+	Cu^{2+}
Band Energy (eV)	933.2	935.6	932.7	934.9
FWHM	1.93	3.0	1.85	2.9
Area	7142	79156	53694	4939
Cu^+/Cu^{2+}	0.09		10.87	

It can be seen form Table 2, both samples 1 and 5 after PC experiments have two kinds of surface state Cu^+ and Cu^{2+}. The ratio of the area of the peaks denotes the relative amount of Cu^+ to Cu^{2+} on the surface. The peak area ratio of Cu^+ to Cu^{2+} on the surface for samples 1 and 5 are 0.09 and 10.87, respectively, indicating that the Cu^{2+} as main surface state exists for sample 1 (similar for samples 2 and 3) and the Cu^+ as main surface state exists for sample 5 (similar for sample 4) after PC experiments. The XRD spectra of samples 1-3 before and after the PC experiments also confirm the transformation of Cu_2O to CuO. However, XRD spectra of samples 4 and 5 before and after PC experiments cannot identify the oxidation of Cu_2O to CuO, suggesting that the amount of CuO is too low to be detected by the XRD measurement and only very thin surface layer of Cu_2O was oxidized into CuO for samples 4 and 5 after the PC experiments. The results further confirm that Cu_2O annealed over 400℃ had better stability than that annealed below 400℃.

3.5 Detection of reactive oxygen species (ROSs)

The generation of $^{\bullet}OH$ was detected by the method of photoluminescence (PL) method. Usually, PL intensity was proportional to the amount of produced $^{\bullet}OH$ in solution. A gradual increase in PL intensity of characteristic peaks at about λ = 425 nm was observed (Figure 7a), indicating that the $^{\bullet}OH$

was formed during PC process. XTT is a widely used $^{\bullet}O_2^-$ probe with a high rate constant for reaction of $^{\bullet}O_2^-$. Figure 7b shows no absorption peak at λ = 470 nm was observed, indicating that the $^{\bullet}O_2^-$ was not produced [27]. H_2O_2 production was analyzed photometrically. Figure 7c displays H_2O_2 was produced and its concentration increased at first and became stable with prolonged irradiation time, due to the decomposition of H_2O_2 in parallel with its production [39].

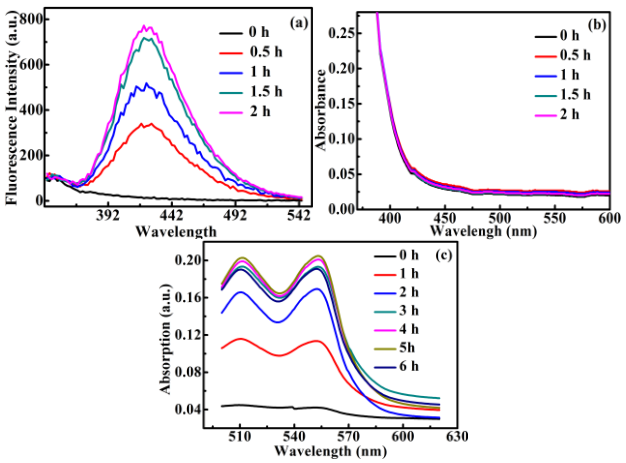

Figure 7 (a) Fluorescence emission spectral changes for the filtrate from the suspension for unannealed Cu_2O with 4×10^{-4} M TA and 2×10^{-3} M NaOH at different time under irradiation (emission at 425 nm, excitation at 315 nm); (b) absorption spectral changes for the filtrate from the suspension with unannealed Cu_2O and 1×10^{-4} M XTT at different time under irradiation (absorption peak 470 nm); (c) absorption spectral of the DPD/POD reagent after reaction with H_2O_2 (absorption peak 551 nm).

3.6 Mechanisms of photocatalysis

The general principle is that when illuminated by light with photoenergy greater than the band gap, the electrons (e^-) of NPs are promoted across the band gap to the conduction band, which creates a hole (h^+) in the valence band. Electrons in the conduction band and holes in the valence band exhibit high reducing and oxidizing power, respectively. The electron can react with molecular oxygen to produce $^{\bullet}O_2^-$ through a reductive process. Although $^{\bullet}O_2^-$ is not a strong oxidant, as a precursor for H_2O_2 and $^{\bullet}OH$ also has significant PC implications [27]. The hole can abstract electrons from water and/or hydroxyl ions to generate $^{\bullet}OH$ through an oxidative process [27]. Thus, h^+, $^{\bullet}OH$, H_2O_2 and $^{\bullet}O_2^-$ are considered to be the major reactive species for the PC dye decolorization [40].

Sketch 1 shows the energy level diagram of Cu_2O as well as the events possibly occurring during PC process. Examining the band structure of Cu_2O in Sketch 1, it can be concluded that the redox potentials for H_2, $^{\bullet}O_2^-$, O_2 and H_2O_2 evolution, the oxidation of Cu_2O to CuO and the reduction of Cu_2O to Cu, are all within the band gap, and therefore, all of these processes are possible, in principle. However, not all the reactions are kinetically favorable, for example, the driving force for water oxidation is minimal, while the oxidation of Cu_2O is thermodynamically favorable [21]. Thus, we have to identify which reactions are available both kinetically and thermodynamically according to the experimental results. Then, we can further analyze the roles of electron, hole, and ROSs for PC process.

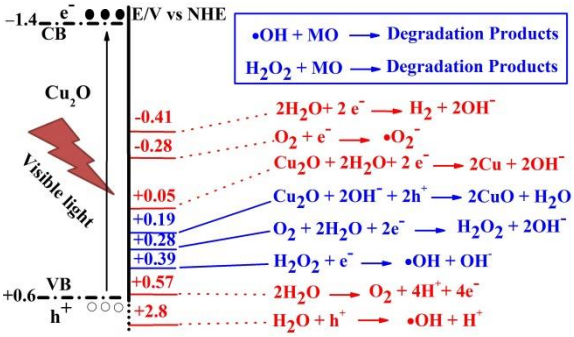

Sketch 1 Energy level diagram of Cu_2O and the events possibly occurring during PC process.

Cu_2O is one of the semiconductors with the highest conduction bands. The band gap of Cu_2O NPs was determined as 2.02 eV in this work, and the potential of its conduction band is −1.4 V (vs. NHE, the same below) [41]. When Cu_2O NPs are irradiated by VL, electrons are separated from holes (Equation 5).

$$Cu_2O + h\nu \rightarrow Cu_2O\,(e^-) + Cu_2O\,(h^+) \quad (5)$$

Thus, those photogenerated electrons with high energy in the conduction band of Cu_2O, besides recombining with holes (Equation 6) or reducing Cu_2O to Cu (which happens at +0.05 V (Equation 7)) [21], are likely to transfer to surface of Cu_2O to react with molecular oxygen to produce $^{\bullet}O_2^-$, H_2O_2 and $^{\bullet}OH$.

$$Cu_2O\,(e^-) + Cu_2O\,(h^+) \rightarrow \text{heat} \quad (6)$$

$$Cu_2O + 2H_2O + 2e^- \rightarrow 2Cu + 2OH^- \quad (7)$$

However, the reduction Cu_2O to Cu by photogenerated electrons unlikely occurred according to our XPS data. Photogenerated electrons also unlikely react with molecular oxygen to produce $^{\bullet}O_2^-$ (Equation 8) because $^{\bullet}O_2^-$ was not detected during our PC experiments.

$$O_2 + e^- \rightarrow {}^{\bullet}O_2^- \quad (8)$$

As for the hole, which is produced at about +0.6 V potential, no overpotential is available for the oxidation of water (about +0.57 V, Equation 9) [42]. It also cannot oxidize H_2O and OH^- to form H_2O_2 (+1.763 V) and $^{\bullet}OH$ (about +2.8 V), respectively. However, the oxidation of the Cu_2O by the hole is favorable (+0.19 V, Equation 10) [43], which was supported by our XRD and XPS data before and after the PC experiments.

$$2H_2O \rightarrow O_2 + 4H^+ + 4e^- \quad (9)$$

$$Cu_2O + 2OH^- + 2h^+ \rightarrow 2CuO + H_2O \quad (10)$$

Since H_2O_2 and $^{\bullet}OH$ signal was detected in our PC process and hole is not their origin, electrons should be responsible for the production of both H_2O_2 and $^{\bullet}OH$ by possible reductive reaction processes. The reductive reaction for production of H_2O_2 can proceed as the cited publication [44] reported: the photogenerated electron is likely to react with molecular oxygen to produce superoxide anion ($^{\bullet}O_2^-$) (−0.28V, Equation 8) [12], then to H_2O_2 through a reductive process. However, no $^{\bullet}O_2^-$ signal was detected in our experiments, so the H_2O_2 came from the direct reduction of O_2 (+0.28 V, Equation 11), which was more thermodynamically available [2, 45]. H_2O_2 can discolor MO with a low degradation rate even in dark [46], suggesting that H_2O_2 is involved in the decolorization of MO during the PC process. Moreover, H_2O_2 is an electron capture, which can capture photogenerated electrons and result in the evolution of $^{\bullet}OH$ according to the Equation 12 [47, 48].

$$O_2 + 2H_2O + 2e^- \rightarrow H_2O_2 + 2OH^- \quad (11)$$

$$H_2O_2 + e^- \rightarrow {}^{\bullet}OH + OH^- \quad (12)$$

Indeed, the process was available because •OH signal was detected in our PC process. •OH is a strong and nonselective oxidant [45] that can result in the decolorization of MO. So, both H_2O_2 and •OH are responsible for the degradation of MO during the PC process.

Conclusions

A fast and simplified synthesis of Cu_2O NPs with highly oriented (111) plane can be achieved by a chemical deposition method with an inorganic process at ambient temperature. The annealing of Cu_2O NPs shows that the higher the annealing temperature, the more highly oriented (111) planes could be formed with increasing annealing temperature. However, when heating Cu_2O at 600 ℃ for 2 h in N_2 atmosphere, a phase transformation happened and the coexistence of Cu_2O and Cu was observed. The Cu_2O NPs show high BET surface areas and a blue shift of absorption edge compared to Cu_2O microparticles. The superior PC activity of Cu_2O NPs may result from its small particle size, high BET surface areas and highly (111) plane oriented crystal composition. However, Cu_2O NPs are more vulnerable to photocorrosion than Cu_2O microparticles. Cu_2O annealed over 400℃ shows better stability than that annealed below 400℃, which might be due to more highly oriented (111) plane for Cu_2O microparticles than nanoparticles. H_2O_2 and •OH played a key role for the degradation of MO during the PC process.

Acknowledgements

This work was supported by the National Natural Science Foundation of China (Grant nos. 61370223 and 51303048), the Natural Science Foundation of Hubei Province (Grant No. 2014CFB579), Hubei Key Laboratory of Quality Control of Characteristic of Fruits and Vegetables, Hubei Engineering University (Grant No. 2014K11 and SWZ009), and Hubei Provincial Department of Education (Grant No. B2014025).

Notes and references

[a]*School of Physics and electronic-information Engineering, Hubei Engineering University, Xiaogan, 432000, China*.
E-Mail: Xiong_lb@yahoo.com, Tel:+86-712-234-5441;
E-Mail: yuhuaqing@126.com, Tel:+86-712-234-5441.
[b]*Key Laboratory of Artificial Micro- and Nano-structures of Ministry of Education of China, School of Physics & Technology, Wuhan University, Wuhan, Hubei 430072, P. R. China.*
[c]*The Institute for Quantum materials and School of Mathematics and Physics Hubei Polytechnic University, Huangshi, P. R. China, 435003, China*.
[d]*College of Chemistry and Materials Science, Hubei Engineering University, Xiaogan 432000, China*

† Electronic Supplementary Information (ESI) available: Photographs of samples 2-5, the peak height/area, peak height/area ratio of planes (111) and (200) of samples 1-5, the UV-vis diffuse reflectance spectra for samples 1, 3, 4 and their corresponding (α Ep)2 vs Ep curves, and XRD patterns of samples 1-5 before and after PC experiments are provided as in ESI. See DOI: 10.1039/b000000x/

1. A. Muramatsu and T. Sugimoto, *J. Colloid Interface Sci.*, 1997, **189**, 167.
2. Y. Chen, T. W. Ng, A. Lu, Y. Li, H. Y. Yip, T. An, G. Li, H. Zhao, M. Gao and P. K. Wong, *Chem. Eng. J.*, 2013, **234**, 43.
3. C. M. Mcshane and K. S. Choi, *Phys. Chem. Chem. Phys.*, 2012, **14**, 6112.
4. C. M. Mcshane, W. P. Siripala and K.-S. Choi, *J. Phys. Chem. L*, 2010, **1**, 2666.
5. J. Y. Xiang, X. L. Wang, X. H. Xia, L. Zhang, Y. Zhou, S. J. Shi and J. P. Tu, *Electrochim. Acta*, 2010, **55**, 4921.
6. S. Sahoo, S. Husale, B. Colwill, T.-M. Lu, S. Nayak and P. M. Ajayan, *ACS Nano*, 2009, **3**, 3935.
7. C. C. Hu, J. N. Nian and H. Teng, *Sol. Energy Mater. Sol. Cells*, 2008, **92**, 1071.
8. M. K. I. Senevirathna, P. K. D. D. P. Pitigala and K. Tennakone, *J. Photochem. Photobiol. A: Chem.*, 2005, **171**, 257.
9. H. Yang and Z.-H. Liu, *Cryst. Growth Des.*, 2010, **10**, 2064.
10. Y. Tan, X. Xue, Q. Peng, H. Zhao, T. Wang and Y. Li, *Nano Lett.*, 2007, **7**, 3723.
11. S. Deki, K. Akamatsu, T. Yano, M. Mizuhata and A. Kajinami, *J. Mater. Chem.*, 1998, **8**, 1865.
12. L. Huang, F. Peng, H. Yu and H. Wang, *Solid State Sci.*, 2009, **11**, 129.
13. H. Liu, W. Miao, S. Yang, Z. Zhang and J. Chen, *Cryst. Growth Des.*, 2009, **9**, 1733.
14. X. Hong, G. Wang, W. Zhu, X. Shen and Y. Wang, *J. Phys. Chem. C*, 2009, **113**, 14172.
15. K. Borgohain, N. Murase and S. Mahamuni, *J. Appl. Phys.*, 2002, **92**, 1292.
16. A. J. Maira, K. L. Yeung, C. Y. Lee, P. L. Yue and C. K. Chan, *J. Catal.*, 2000, **192**, 185.
17. C. H. Kuo and M. H. Huang, *J. Am. Chem. Soc.*, 2008, **130**, 12815.
18. Y. Xu, H. Wang, Y. Yu, L. Tian, W. Zhao and B. Zhang, *J. Phys. Chem. C*, 2011, **115**, 15288.
19. Z. Zheng, B. Huang, Z. Wang, M. Guo, X. Qin, X. Zhang, P. Wang and Y. Dai, *J. Phys. Chem. C*, 2009, **113**, 14448.
20. K. L. Sowers and A. Fillinger, *J. Electrochem. Soc.*, 2009, **156**, F80.
21. L. Wu, L. Tsui, N. Swami and G. Zangari, *J. Phys. Chem. C*, 2010, **114**, 11551.
22. L. Xiong, H. Yu, G. Yang, M. Qiu, J. Chen and Y. Yu, *Thin Solid Film.*, 2010, **518**, 6738.
23. A. Paracchino, N. Mathews, T. Hisatomi, M. Stefik, S. D. Tilley and M. Grätzel, *Energy Environ. Sci.*, 2012, **5**, 8673.
24. R. J. Mohd, S. M. S. Mohd, L. H. Nor and A. C. Hee, *Int. J. Electrochem. Sci*, 2011, **6**, 6094.
25. W. Siripala, L. D. R. D. Perera, K. T. L. De Silva, J. K. D. S. Jayanetti and I. M. Dharmadasa, *Sol. Energy Mater. Sol. Cells*, 1996, **44**, 251.
26. K. Ishibashi, A. Fujishima, T. Watanabe and K. Hashimoto, *J. Photochem. Photobiol. A: Chem.*, 2000, **134**, 139.
27. Y. Li, W. Zhang, J. Niu and Y. Chen, *ACS Nano*, 2012, **6**, 5164.
28. H. Bader, V. Sturzenegger and J. Hoigné, *Water Res.*, 1988, **22**, 1109.
29. W. Wang, Y. Yu, T. An, G. Li, H. Y. Yip, J. C. Yu and P. K. Wong, *Environ. Sci. Technol.*, 2012, **46**, 4599.
30. M.T.S. Nair, L. Guerrero, O. L. Arenas and P. K. Nair, *Appl. Surf. Sci.*, 1999, **150**, 143.
31. N. Yang, Z. Wang, L. Chen, Y. Wang and Y. B. Zhu, *Int. J. Refract. Met. Hard Mater.*, 2010, **28**, 198.

32. Y. Nakano, S. Saeki and T. Morikawa, *Appl. Phys. Lett.*, 2009, **94**, 022111.
33. L. Ma, J. Li, H. Sun, M. Qiu, J. Wang, J. Chen and Y. Yu, *Mater. Res. Bull.*, 2010, **45**, 961.
34. M. Yin, C.K. Wu, Y.B. Lou, C. Burda, J.T. Koberstein, Y.M. Zhu and S. O'brien, *J. Am. Chem. Soc.*, 2005, **127**, 9506.
35. C. A. Martín, M. A. Baltanás and A. E. Cassano, *J. Photochem. Photobiol. A: Chem.*, 1993, **76**, 199.
36. H. Xu, W. Wang and W. Zhu, *J. Phys. Chem. B*, 2006, **110**, 13829.
37. X. Zhang, J. Song, J. Jiao and X. Mei, *Solid State Sci.*, 2010, **12**, 1215.
38. T. Ghodselahi, M. A. Vesaghi, A. Shafiekhani, A. Baghizadeh and M. Lameii, *Appl. Surf. Sci.*, 2008, **255**, 2730.
39. F. Shiraishi and C. Kawanishi, *J. Phys. Chem. A*, 2004, **108**, 10491.
40. W. Wang, L. Zhang, T. An, G. Li, H. Yip and P. Wong, *Appl. Catal. B: Environ.*, 2011, **108-109**, 108.
41. L. Xiong, M. Ouyang, L. Yan, J. Li, M. Qiu and Y. Yu, *Chem. Lett.*, 2009, **38**, 1154.
42. P. E. De Jongh, D. Vanmaekelbergh and J. J. Kelly, *J. Electrochem. Soc.*, 2000, **147**, 486.
43. P. E. De Jongh, D. Vanmaekelbergh and J. J. Kelly, *Chem. Commun.*, 1999, 1069.
44. H. Lin, S. Liao and S. Hung, *J. Photochem. Photobiol. A: Chem.*, 2005, **174**, 82.
45. Y. Zhang, L. Ma, J. Li and Y. Yu, *Environ. Sci. Technol.*, 2007, **41**, 6264.
46. M. Azami, M. Bahram, S. Nouri and A. Naseri, *J. Serb. Chem. Soc.*, 2012, **77**, 235.
47. H. Yang, K. Zhang, R. Shi, X. Li, X. Dong and Y. Yu, *J. Alloys Compd.*, 2006, **413**, 302.
48. H. K. Willem, M. S. David and L. B. Patricia, *Free Radical Biol. Med.*, 2010, **49**, 317.

